coatings

MDPI

Communication

Enhanced Thermoelectric Properties of Sb_2Te_3 Thin Films by In Doping

Meng Wei [1], Yiming Zhong [1], Gaiqing Zhao [1,*], Ping Fan [1], Dongwei Ao [2,3], Zhuanghao Zheng [1] and Yuexing Chen [1,*]

[1] Shenzhen Key Laboratory of Advanced Thin Films and Applications, Key Laboratory of Optoelectronic Devices and Systems of Ministry of Education and Guangdong Province, College of Physics and Optoelectronic Engineering, Shenzhen University, Shenzhen 518060, China; mengwei@szu.edu.cn (M.W.); 15367480096@163.com (Y.Z.); fanping@szu.edu.cn (P.F.); zhengzh@szu.edu.cn (Z.Z.)
[2] School of Machinery and Automation, Weifang University, Weifang 261061, China; aodongwei@wfu.edu.cn
[3] College of Chemical Engineering, Tianjin University, Tianjin 300072, China
* Correspondence: zhaogq@szu.edu.cn (G.Z.); chenyx@szu.edu.cn (Y.C.)

Abstract: Flexible Sb_2Te_3-based thermoelectric (TE) materials are promising candidates for fabricating energy devices that power wearable electronics and sensors. Enhancing the TE properties of Sb_2Te_3 thin films represents a significant scientific investigation. In this work, a thermal diffusion method is applied to prepare the In-doped Sb_2Te_3 thin film. In doping can lead to a high Seebeck coefficient of ~137.04 μV K^{-1} as well as moderate electrical conductivity. As a result, the high power factor of ~18.22 μW cm^{-1} K^{-2} at 303 K is achieved. Moreover, In doping could reduce the thermal conductivity owing to the increase in phonon scattering. Finally, the high ZT values of ~0.47 at room temperature (303 K) and ~0.6 at 453 K are obtained. This indicates that In doping is a highly promising and effective approach to improving the TE performance of Sb_2Te_3 thin films.

Keywords: thermoelectric; Sb_2Te_3 thin films; In doping; thermoelectric properties

Citation: Wei, M.; Zhong, Y.; Zhao, G.; Fan, P.; Ao, D.; Zheng, Z.; Chen, Y. Enhanced Thermoelectric Properties of Sb_2Te_3 Thin Films by In Doping. *Coatings* **2023**, *13*, 1784. https://doi.org/10.3390/coatings13101784

Academic Editor: Ihor S. Virt

Received: 21 September 2023
Revised: 10 October 2023
Accepted: 16 October 2023
Published: 17 October 2023

1. Introduction

With the growing demand for providing the power for wearable micro-electronic devices or the Internet of Things, high-performance micro-scale power generators are in increasingly high demand [1–4]. Thermoelectric (TE) materials have been extensively studied for their ability to convert thermal energy into electrical energy [5,6]. TE devices offer a sustainable, reliable power supply with efficient energy harvesting from complex geometric surfaces, including the human body [7]. The efficiency of the TE devices typically depends on the figure of merit (ZT) value, $ZT = S^2\sigma T/\kappa$, where S, σ, T, and κ ($\kappa = \kappa_l + \kappa_e$) signify Seebeck coefficient, electrical conductivity, absolution temperature, and total thermal conductivity (κ_e and κ_l are electronic thermal conductivity and lattice thermal conductivity), respectively. Obviously, a higher ZT value can be attained through an increase in $S^2\sigma$ and a decrease in κ, where $S^2\sigma$ represents the power factor (PF) [8,9]. And an optimized $S^2\sigma$ can be obtained by tuning carrier concentration. Meanwhile, a low κ_l can be achieved by optimizing structural designs.

Thin-film TE materials are currently a research hotspot due to their greater potential for powering wearable electronics devices. Among many the state-of-the-art TE materials, p-type Sb_2Te_3 has attracted much attention owing to its excellent TE performance around room temperature. Several deposition technologies to enhance TE performance have been investigated, such as magnetron sputtering [10], vacuum thermal evaporation [11,12], pulsed laser deposition (PLD) [13], molecular beam epitaxy [14], screen printing [15], and electrochemical deposition method [16]. Vieira et al. [17] deposited Sb_2Te_3 thin film on flexible (polyimide, PI) substrate by a thermal evaporation method, and the $S^2\sigma$ of ~12.0 μW cm^{-1} K^{-2} at 298 K was achieved. Wu et al. [18] used a co-sputtering technology

to obtain Sb_2Te_3/Te thin film with a $S^2\sigma$ of ~11.2 μW cm^{-1} K^{-2} at room temperature. Kong et al. [19] carried out a magnetron sputtering method to prepare a Sb_2Te_3 flexible thin film with an optimal $S^2\sigma$ of 17.5 μW cm^{-1} K^{-2} at room temperature. Shang et al. [20] achieved a $S^2\sigma$ of 12.4 μW cm^{-1} K^{-2} at 300 K in flexible $Bi_{0.5}Sb_{1.5}Te_3$-based films and further improved the $S^2\sigma$ of 23.2 μW cm^{-1} K^{-2} at 300 K using a facile approach that involves introducing the Te and Sb_2Te_3 nanoinclusions [21]. The intrinsic TE performance of Sb_2Te_3 is insufficient to meet practical application requirements, and further enhancing the thermoelectric properties is necessary.

Doping has been scientifically proven to be an effective method for enhancing the TE properties of materials by manipulating carrier concentration to regulate electrical conductivity and the Seebeck coefficient. Argemi et al. [22] achieved a high $S^2\sigma$ of 18.7 μW cm^{-1} K^{-2} for $Ag_{3.9}Sb_{33.6}Te_{62.5}$ by optimizing Ag doping. With co-doping of Ag/In in Sb_2Te_3, enlarged E_g was observed, which yielded a ZT of ~1 at 673 K [23]. Hu et al. [24] increased carrier concentration by coordinating the ratio of Bi/Sb and obtained a high ZT of ~1.3 at 373 K in $Bi_{0.3}Sb_{1.7}Te_3$. Additionally, In has also been frequently considered as a doping element in Sb_2Te_3, which may lead to intrinsic vacancies with the high density at cation sites owing to the lattice mismatch between indium (In^{3+}) (In^{3+} is supposed to substitute Sb^{3+}) and tellurium ions (Te^{2-}) [25,26]. Therefore, TE performance should be enhanced via phonon-vacancy scattering, which plays a substantial role in reducing thermal conductivity [27–29]. In summary, In is a promising doping element for improving the TE properties of the Sb_2Te_3 thin film.

In this work, we aim at successfully preparing Sb_2Te_3 thin film using a simple deposition method that facilitates rapid and simple deposition on large, flexible surfaces. The thin film composition could be easily adjusted by controlling the thickness of each film. It will lay the foundation for the following doping research. In order to further enhance the thermoelectric properties of intrinsic thin films and explore more in-depth mechanisms, the effect of In doping on the properties of *p*-type Sb_2Te_3 flexible TE thin film has been investigated. Through the analysis of the microstructure of the prepared thin films and the combined theoretical calculation analysis, it is proved that the In doping can eventually lead to achieving enhanced thermoelectric properties. Especially the ZT value of ~0.6 at 453 K was obtained in In-doped Sb_2Te_3, which is approximately 1.5 times higher than that of undoped Sb_2Te_3 thin film. This indicates In doping is an effective and promising method to improve the TE properties of Sb_2Te_3 thin films.

2. Materials and Methods

A flexible polyimide substrate with a low thermal conductivity of 0.12 W K^{-1} m^{-1} was selected and directed at the deposition of Sb and Te thin films. The substrates were cleaned in an ultrasonic bath for 10 min with absolute ethyl alcohol, then for 10 min with deionized water. The Sb was prepared via direct current (DC) magnetron sputtering, while the Te and In were deposited using radio frequency (RF) magnetron sputtering. The parameters of deposition for Te thin films were as follows: a sputtering power of 20 W during 42 min, an argon flow of 40 sccm, and a working pressure of 0.7 Pa. The deposition parameters of In-doped Sb thin films were as follows: Sb and In sputtering power of 20 W and 10 W, Sb and In sputtering time of 23 min and 3 min, respectively, and the working pressure of 0.7 Pa. In-doped Sb_2Te_3 thin film was prepared by thermal diffusion at 623 K. Based on In doping, the samples are marked as In $_{0\ at.\%}$ and In $_{0.98\ at.\%}$.

Crystal structural formations were detected and analyzed by X-ray diffraction (XRD, D/max 2500, Rigaku Corporation, Tokyo, Japan) with the θ-2θ mode using the incident angle of 20–80° (Cu/Kα, 40 kV). Raman scattering measurements were implemented by the Micro-Raman Spectroscopy System (RENISHAW inVia, Gloucestershire, UK). X-ray photoelectron spectroscopy (XPS, Thermo ESCALAB 250XI, Waltham, MA, US) was carried out to investigate the chemical valence states of elements. Surface and cross-sectional morphology were performed by scanning electron microscopy (SEM, Zeiss supra 55, Carl Zeiss, Oberkochen, Germany), while chemical content analysis was analyzed by energy dispersive

spectroscopy (EDS, Quantax, Bruker, Karlsruhe, Germany). The σ and S were measured by the TE performance measurement system (Netzsch SBA458, Netzsch, Shanghai, China) at a temperature of 303–453 K. The room temperature carrier concentration (n) and mobility (μ) were characterized using the Hall measurement system (HL5500PC, Nanometrics, Milpitas, CA, USA). The thicknesses of the thin films were tested by the surface-profile measurement system (Bruker Dektak XT, Bruker, Karlsruhe, Germany). The values of thermal conductivity κ were measured by the transient electrothermal technique [30]. The errors of the parameters were as follows: S, σ, and κ are 7%, 7%, and 10%, respectively.

3. Results and Discussion

Figure 1a,d display the SEM surface morphology of In $_{0\ at.\%}$ and In $_{0.98\ at.\%}$ thin films. Uniform and denseness of the film surface can be observed for In $_{0\ at.\%}$ thin film, and there are no obvious void defects. The In $_{0.98\ at.\%}$ thin film shows a clearly quite rough surface, which is mightily attributed to the internal stress resulting from In doping. The cross-sectional images in Figure 1c,d present that the In doping can significantly increase the grain size. The EDS mapping of the sample In $_{0.98\ at.\%}$ shown in Figure 1e–h demonstrates the homogenous distribution of all the constituting elements. The EDS results are shown in Table 1. The corresponding thicknesses of the In $_{0\ at.\%}$ and In $_{0.98\ at.\%}$ thin films were 680 and 700 nm, respectively. The thickness of ~700 nm for In $_{0.98\ at.\%}$ thin films is owing to the large grain size, as can be seen in Figure 1d. The atomic ratio of Sb/Te for the In $_{0\ at.\%}$ tin film is close to 2:3, acquired by regulating the thickness of Sb and Te thin films. The proportion of In-doped samples changes due to the influence of In doping elements.

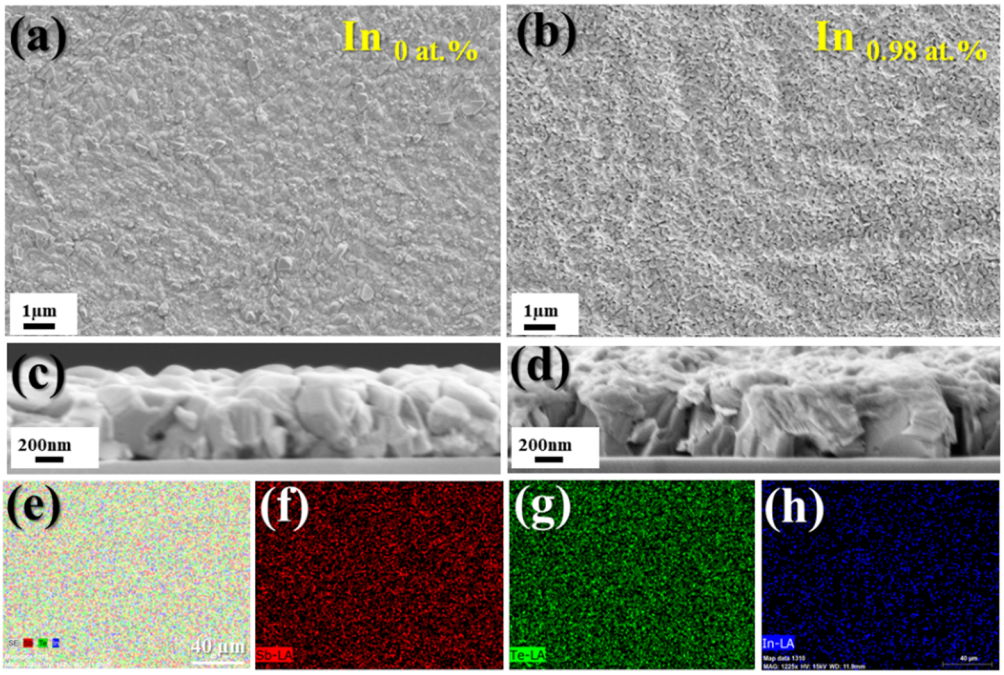

Figure 1. (**a**,**b**) SEM images of the top view of In $_{0\ at.\%}$ and In $_{0.98\ at.\%}$ thin film. (**c**,**d**) The cross-section images of the In $_{0\ at.\%}$ and In $_{0.98\ at.\%}$ thin films. (**e**–**h**) EDS mapping for the Sb, Te, and In elements of In $_{0.98\ at.\%}$ thin film.

Table 1. The chemical content, thicknesses, μ and n of undoped and In-doped Sb_2Te_3 thin films.

Sample	Sb (at.%)	Te (at.%)	In (at.%)	Thickness (nm)	μ ($cm^2\ V^{-1}\ s^{-1}$)	n ($\times 10^{19}\ cm^{-3}$)
Undoped	38.90	61.10	0	680	240.72	3.2
In-doped	41.63	57.39	0.98	700	126.14	4.8

Figure 2a exhibits the XRD patterns of the In $_{0\ at.\%}$ and In $_{0.98\ at.\%}$ thin films, which can be essentially indexed to the standard peaks of Sb_2Te_3 (PDF #15-0874). The (101) peak of Te can be suspected in In $_{0\ at.\%}$ thin film; however, it is not really visible in In $_{0.98\ at.\%}$ thin film. Therefore, In doping appears to inhibit Te precipitation in the Sb_2Te_3 thin film. Room-temperature Raman scattering measurements were executed using the Micro-Raman Spectroscopy System (Figure 2b). As supposed, there are five atoms per unit cell in Sb_2Te_3 for two-dimensional, thus each wavevector K exhibits 15 phonon modes. Theoretical analysis for K = 0 is the following: $\Gamma_{Raman} = 2A_{1g} + 2E_g$ [31,32]. There are three Raman-sensitive phonon vibration modes for the Sb_2Te_3 single crystal in the range of 55 to 210 cm^{-1}. Here, three typical Sb_2Te_3 Raman modes are visible, located at 70.0 cm^{-1}, 111.3 cm^{-1}, and 165.9 cm^{-1}, which are in accordance with the $A^1{}_{1g}$, $E^2{}_g$, and $A^2{}_{1g}$, respectively. For the In-doping sample, the Raman shift has slightly shifted, possibly due to the In-doping.

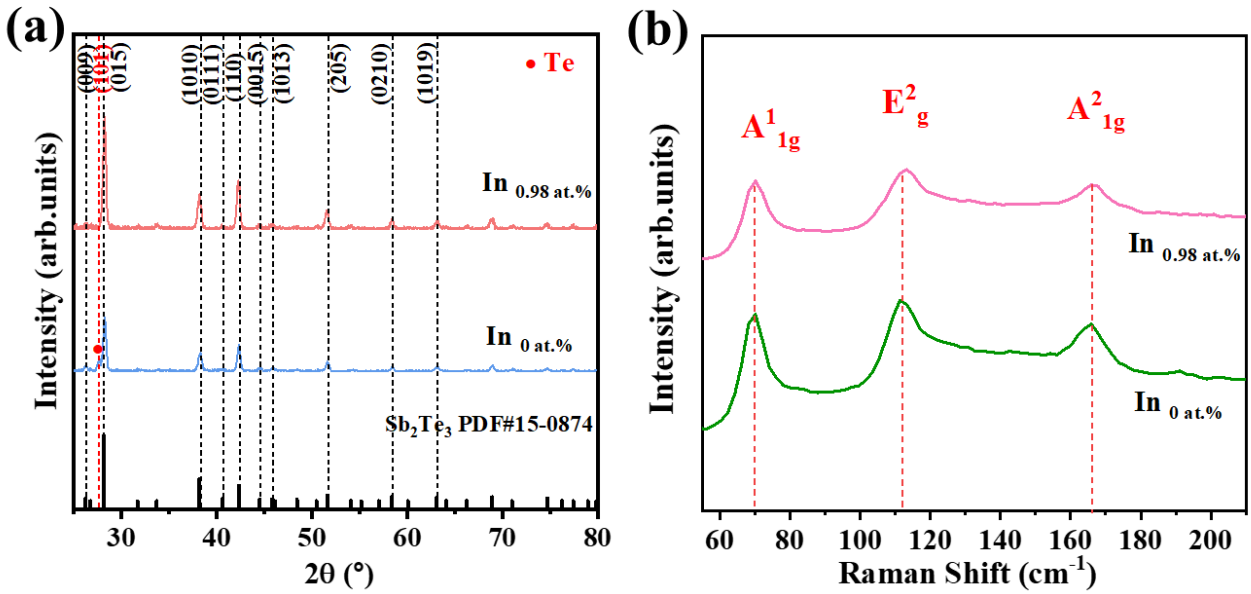

Figure 2. (**a**) X-ray diffraction (XRD) patterns and (**b**) Raman spectra of In $_{0\ at.\%}$ and In $_{0.98\ at.\%}$ thin films.

To further analyze the microstructures of the Sb_2Te_3 thin film, the chemical valence was carried out by XPS, as shown in Figure 3. The spectra of the Sb 3d, Te 3d, and In 3d were obtained, as shown in Figure 3a, which uses the C1s as the calibration reference at 284.8 eV. The binding energies were obviously detected, which correspond to the energy levels of Sb, Te, and In. As shown in Figure 3b, the binding energies at 529.88 eV and 537.28 eV are consistent with Sb $3d_{5/2}$ and Sb $3d_{3/2}$, confirming the Sb^{3+} valence state. In Figure 3c, the binding energies at 582.08 eV and 571.68 eV are consistent with the Te $3d_{3/2}$ and Te $3d_{5/2}$, confirming the Te^{2-} valence states. Some impurities, including an oxygen peak, were observed due to the absence of plasma etching to remove the surface impurities. The peak of O 1s at ~531.78 eV in Figure 3b corresponds to Sb_2O_3, while the peak of O 1s at ~587.68 eV in Figure 3c refers to TeO_3 [33]. The binding energy of In $3d_{5/2}$ is located at ~443.58 eV and In $3d_{3/2}$ is located at ~451.28 eV, confirming the In^{3+} valence state (Figure 3d). It indicated that In was introduced into the cationic sites of Sb_2Te_3, which may replace Sb.

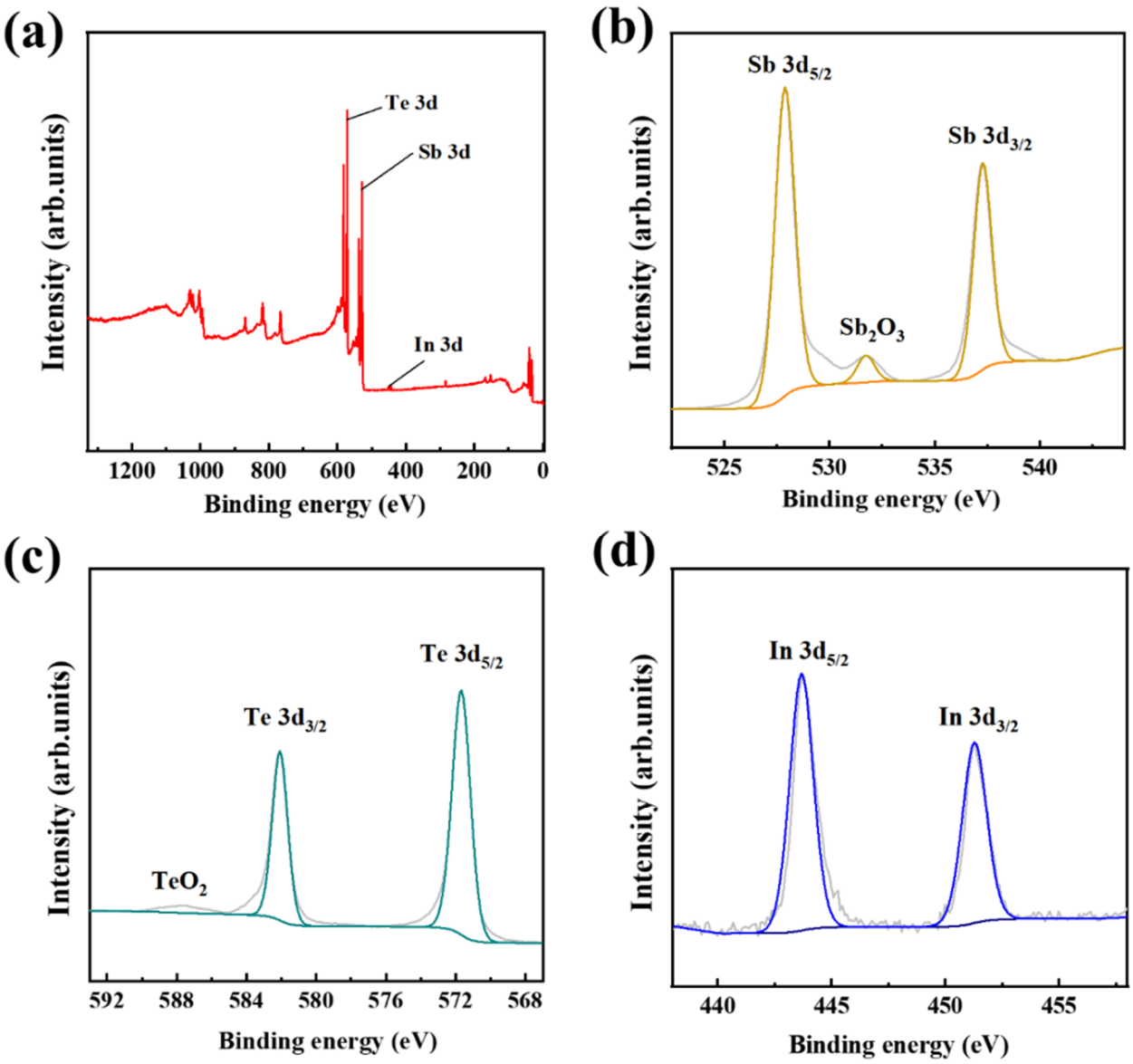

Figure 3. (**a**) XPS full spectrum. The XPS spectra of (**b**) Sb 3d, (**c**) Te 3d, and (**d**) In 3d of the In $_{0.98\ at.\%}$ thin film.

Figure 4a–c shows the temperature dependence of TE performance (σ, S, and $S^2\sigma$) in In $_{0\ at.\%}$ and In $_{0.98\ at.\%}$ thin films. Both σ decreased with increasing temperature, as shown in Figure 4a. Correspondingly, the maximum room-temperature σ is achieved for the In $_{0\ at.\%}$ and In $_{0.98\ at.\%}$ thin films. The σ of the In $_{0.98\ at.\%}$ thin film is lower than that of the In $_{0\ at.\%}$ thin film, as shown in Figure 4a. To further understand the electric performance evaluation, Hall performance was investigated in Table 1. The μ values of In $_{0.98\ at.\%}$ thin film are lower than those of In $_{0\ at.\%}$. As can be seen, the high σ of In $_{0\ at.\%}$ is attributed to the high μ. The effective mass (m^*) and deformation potential (E_{def}) in In $_{0\ at.\%}$ and In $_{0.98\ at.\%}$ thin film calculations are presented in Figure 4d. The m^* and E_{def} are calculated via a single parabolic band (SPB) model based on density-functional-theory [34]. The high μ is mainly due to the low E_{def}. Figure 4b shows the comparison of S of In $_{0\ at.\%}$ and In $_{0.98\ at.\%}$ thin film. The S increased with increasing temperature for In $_{0\ at.\%}$ and In $_{0.98\ at.\%}$ thin films. And S of In $_{0.98\ at.\%}$ thin film is higher than that of In $_{0\ at.\%}$ thin film. The maximum S value of ~137.04 μV K^{-1} is achieved in In $_{0.98\ at.\%}$ at 303 K. The high S of In $_{0.98\ at.\%}$ thin film is mainly attributed to the high m^*, but regardless of the high n as shown in Table 1. Figure 4c presents the $S^2\sigma$ as a function of temperature in In $_{0\ at.\%}$ and In $_{0.98\ at.\%}$ thin films. The $S^2\sigma$ decreased

with increasing temperature. The higher $S^2\sigma$ of In $_{0.98\ at.\%}$ thin film is achieved compared with In $_{0\ at.\%}$ thin film. The highest $S^2\sigma$ of 18.22 μW cm^{-1} K^{-2} at 303 K is achieved due to the high S and a moderate σ of In $_{0.98\ at.\%}$ thin film. Additionally, the fitted n-dependent $S^2\sigma$ was calculated with the single parabolic band model and experimental $S^2\sigma$ at room temperature as shown in Figure 4d. It is indicated that the high $S^2\sigma$ should be mainly attributed to the tuning n close to the optimal level (~1 × 10^{19} cm^{-3} to ~1 × 10^{20} cm^{-3}).

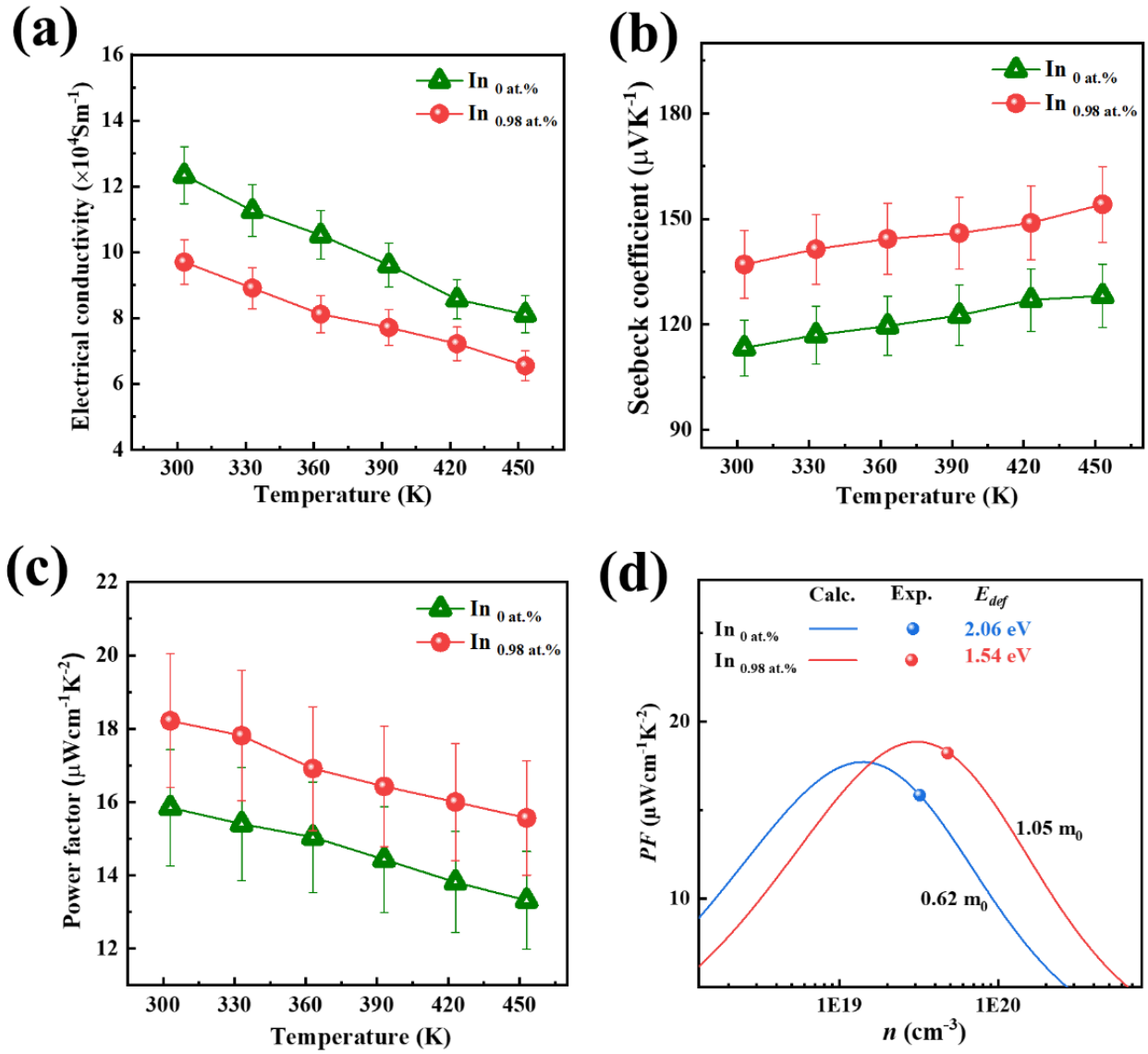

Figure 4. (**a**) σ, (**b**) S, and (**c**) $S^2\sigma$ (PF) as a function of temperature in In $_{0\ at.\%}$ and In $_{0.98\ at.\%}$ thin film. (**d**) The $n-$dependent measured and SPB-model calculated $S^2\sigma$ at room temperature.

To further investigate the influence of the In-doping effect on the TE properties of the thin films, the room temperature (303 K) thermal conductivity (κ) was measured. Figure 5a presents a schematic illustration of measuring the thermal conductivity κ of a Sb_2Te_3-based thin film. The measurement method of κ is the transient electrothermal technique [35,36]. The temperature evolution history can be used to calculate the thermal diffusivity of In $_{0\ at.\%}$ and In $_{0.98\ at.\%}$ thin films [35,37]. And the κ of 1.18 W m^{-1} K^{-1} for In $_{0.98\ at.\%}$ thin film is obtained, which is lower than that of In $_{0\ at.\%}$ thin film. It is indicated In doping could decrease the κ of the Sb_2Te_3 thin film, as shown in Figure 5b. The In doping could create more phonon scattering centers in the lattice, leading to a decrease in κ. The doping of In may also introduce more lattice defects or grain boundaries, which could cause a decrease

in thermal conductivity. Finally, the dependence of temperature on the *ZT* value is also shown in Figure 5b. The *ZT* values of ~0.47 at room temperature (303 K) and ~0.6 at 453 K are obtained in In $_{0.98\ at.\%}$ thin film, which is higher than that of undoped thin film. As a result, In doping has great potential for improving TE performance due to the high $S^2\sigma$ and low κ.

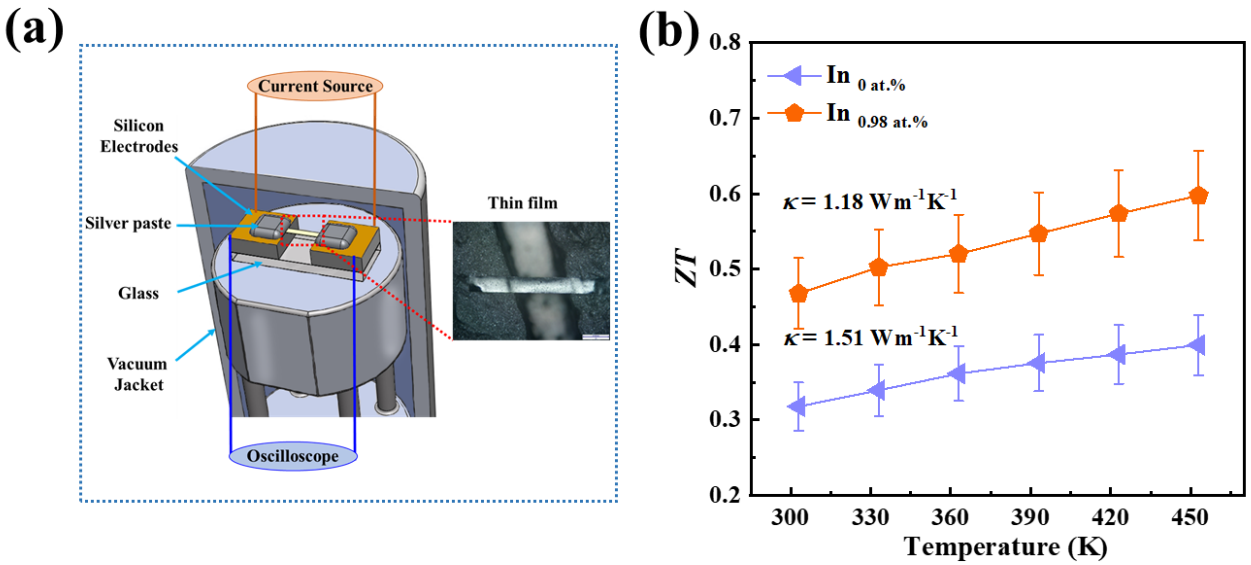

Figure 5. (**a**) A schematic illustration of measuring the κ process. (**b**) *ZT* values for In $_{0\ at.\%}$ and In $_{0.98\ at.\%}$ thin film.

4. Conclusions

In summary, In $_{0\ at.\%}$ and In $_{0.98\ at.\%}$ Sb_2Te_3 thin films were successfully fabricated by an innovative thermally induced diffusion reaction. In doping could increase the Seebeck coefficient to ~137.04 μV K^{-1}, due to the high m^*. Meanwhile, tuning n optimizes it to an optimal level. As a result, it leads to a high power factor of ~18.22 μW cm^{-1} K^{-2} at 303 K. Correspondingly, the thermal conductivity of In $_{0.98\ at.\%}$ thin film is 1.18 W m^{-1} K^{-1} owing to the increase of phonon scattering and lattice or grain boundary defects. Consequently, a high *ZT* value of ~0.47 at room temperature (303 K) and ~0.6 at 453 K is achieved due to the high power factor and low thermal conductivity. This work indicates In doping can enhance the thermoelectric properties of the Sb_2Te_3−based thin film.

Author Contributions: Made substantial contributions to conceptualization and design of methodology and writing—original draft: M.W. and Y.Z. Provided administration: Z.Z. and Y.C. Supervision and Funding acquisition: Z.Z. Performed data acquisition as well as, technical, and writing—review and editing: P.F., D.A., Z.Z., G.Z. and Y.C. All authors have read and agreed to the published version of the manuscript.

Funding: This work was supported by the National Natural Science Foundation of China (No. 62274112) and the Guangdong Basic and Applied Basic Research Foundation (2022A1515010929).

Institutional Review Board Statement: Not applicable.

Informed Consent Statement: Not applicable.

Data Availability Statement: Not applicable.

Conflicts of Interest: The authors declare no conflict of interest.

References

1. Harman, T.C.; Taylor, P.J.; Walsh, M.P.; LaForge, B.E. Quantum dot superlattice thermoelectric materials and devices. *Science* **2002**, *297*, 22292232. [CrossRef] [PubMed]
2. Ao, D.W.; Liu, W.D.; Chen, Y.X.; Wei, M.; Jabar, B.; Li, F.; Shi, X.L.; Zheng, Z.H.; Liang, G.X.; Zhang, X.H.; et al. Novel thermal diffusion temperature engineering leading to high thermoelectric performance in Bi_2Te_3-based flexible thin-films. *Adv. Sci.* **2022**, *9*, 2103547. [CrossRef] [PubMed]
3. Shi, X.L.; Zou, J.; Chen, Z.G. Advanced thermoelectric design, from materials and structures to devices. *Chem. Rev.* **2020**, *120*, 7399–7515. [CrossRef] [PubMed]
4. Xiao, Y.; Zhao, L.D. Seeking new, highly effective thermoelectrics. *Science* **2020**, *367*, 1196–1197. [CrossRef] [PubMed]
5. Wang, Y.; Yang, L.; Shi, X.L.; Shi, X.; Chen, L.D.; Dargusch, M.S.; Zou, J.; Chen, Z.G. Flexible thermoelectric materials and generators, challenges and innovations. *Adv. Mater.* **2019**, *31*, 1807916. [CrossRef] [PubMed]
6. Zhao, Y.; Liu, L.Y.; Zhang, F.J.; Di, C.A.; Zhu, D.B. Advances in organic thermoelectric materials and devices for smart applications. *SmartMat* **2021**, *2*, 426–445. [CrossRef]
7. Fan, Z.; Zhang, Y.Y.; Pan, L.J.; Ouyang, J.Y.; Zhang, Q. Recent developments in flexible thermoelectrics, From materials to devices. *Renew. Sustain. Energy Rev.* **2021**, *137*, 110448. [CrossRef]
8. Singkaselit, K.; Sakulkalavek, A.; Sakdanuphab, R. Effects of annealing temperature on the structural, mechanical and electrical properties of flexible bismuth telluride thin films prepared by high-pressure RF magnetron sputtering. *Adv. Nat. Sci.-Nanosci. Nanotechnol.* **2017**, *8*, 035002. [CrossRef]
9. Kuang, N.; Zuo, Z.; Wang, W.; Liu, R.; Zhao, Z. Optimized thermoelectric properties and geometry parameters of annular thin-film thermoelectric generators using n-type $Bi_2Te_{2.7}Se_{0.3}$ and p-type $Bi_{0.5}Sb_{1.5}Te_3$ thin films for energy harvesting. *Sens. Actuators A Phys.* **2021**, *332*, 113030. [CrossRef]
10. Jeong, M.W.; Na, S.; Shin, H.; Park, H.B.; Lee, H.J.; Joo, Y.C. Thermomechanical in situ monitoring of Bi_2Te_3 thin film and its relationship with microstructure and thermoelectric performances. *Electron. Mater. Lett.* **2018**, *14*, 426–431. [CrossRef]
11. Soliman, L.I.; Nassary, M.M.; Shaban, H.T.; Salwa, A.S. Influence of Se on the electron mobility in thermal evaporated $Bi_2(Te_{1-x}Se_x)_3$. *Thin Film.* **2010**, *85*, 358–364. [CrossRef]
12. Li, Y.Z.; Li, F.; Liang, G.X.; Zheng, W.L.; Xu, Y.M.; Zheng, Z.H.; Fan, P. Sb_2Se_3 thin films fabricated by thermal evaporation deposition using the powder prepared via mechanical alloying. *Surf. Coat. Technol.* **2019**, *358*, 1013–1101. [CrossRef]
13. Makala, R.S.; Jagannadham, K.; Sales, B.C. Pulsed laser deposition of Bi_2Te_3-based thermoelectric thin films. *J. Appl. Phys.* **2003**, *94*, 3907–3918. [CrossRef]
14. Choi, H.; Jeong, K.; Chae, J.; Park, H.; Baeck, J.; Kim, T.H.; Song, J.Y.; Park, J.; Jeong, K.H.; Cho, M.H. Enhancement in thermoelectric properties of Te-embedded Bi_2Te_3 by preferential phonon scattering in heterostructure interface. *Nano Energy* **2018**, *47*, 374–384. [CrossRef]
15. Kim, S.J.; Wea, J.H.; Kim, J.S.; Kim, G.S.; Cho, B.J. Thermoelectric properties of P-type Sb_2Te_3 thick film processed by a screen-printing technique and a subsequent annealing process. *J. Alloys Compd.* **2014**, *582*, 177–180. [CrossRef]
16. Trung, N.H.; Sakamoto, K.; Toan, N.V.; Ono, T. Synthesis and evaluation of thick films of electrochemically deposited Bi_2Te_3 and Sb_2Te_3 thermoelectric materials. *Materials* **2017**, *10*, 154. [CrossRef] [PubMed]
17. Vieira, E.M.F.; Figureueira, J.; Pires, A.L.; Grilo, J.; Silva, M.F.; Pereira, A.M.; Goncalves, L.M. Enhanced thermoelectric properties of Sb_2Te_3 and Bi_2Te_3 films for flexible thermal sensors. *J. Alloys Compd.* **2019**, *774*, 1102–1116. [CrossRef]
18. Wu, Z.H.; Chen, X.; Mu, E.Z.; Liu, Y.; Che, Z.X.; Dun, C.C.; Sun, F.Y.; Wang, X.W.; Zhang, Y.L.; Hu, Z.Y. Lattice strain enhances thermoelectric properties in Sb_2Te_3/Te heterostructure. *Adv. Electron. Mater.* **2020**, *6*, 1900735. [CrossRef]
19. Kong, D.Y.; Zhu, W.; Guo, Z.P.; Deng, Y. High-performance flexible Bi_2Te_3 films based wearable thermoelectric generator for energy harvesting. *Energy* **2019**, *175*, 292–299. [CrossRef]
20. Shang, H.J.; Li, T.G.; Luo, D.; Yu, L.; Zou, Q.; Huang, D.X.; Xiao, L.Y.; Gu, H.W.; Ren, Z.F.; Ding, F.Z. High-performance Ag-modified $Bi_{0.5}Sb_{1.5}Te_3$ films for the flexible thermoelectric generator. *ACS Appl. Mater. Interfaces* **2020**, *12*, 7358–7365. [CrossRef]
21. Shang, H.J.; Dun, C.C.; Deng, Y.; Li, T.G.; Gao, Z.S.; Xiao, L.Y.; Gu, H.W.; Singh, D.J.J.; Ren, Z.F.; Ding, F.Z. $Bi_{0.5}Sb_{1.5}Te_3$-based films for flexible thermoelectric devices. *J. Mater. Chem. A* **2020**, *8*, 4552–4561. [CrossRef]
22. Argemi, L.F.; Yu, Z.Q.; Kim, J.; Myung, N.V.; Lim, J.H.; Lee, J. Silver content dependent thermal conductivity and thermoelectric properties of electrodeposited antimony telluride thin films. *Sci. Rep.* **2019**, *9*, 9242. [CrossRef] [PubMed]
23. Hu, L.P.; Zhu, T.J.; Yue, X.Q.; Liu, X.H.; Wang, Y.G.; Xu, Z.J.; Zhao, X.B. Enhanced figure of merit in antimony telluride thermoelectric materials by In-Ag co-alloying for mid-temperature power generation. *Acta Mater.* **2015**, *85*, 270–278. [CrossRef]
24. Hu, L.P.; Zhu, T.J.; Wang, Y.G.; Xie, H.H.; Xu, Z.J.; Zhao, X.B. Shifting up the optimum figure of merit of P-type bismuth telluride-based thermoelectric materials for power generation by suppressing intrinsic conduction. *NPG Asia Mater.* **2014**, *6*, 88. [CrossRef]
25. Popov, I.U.M.; Popov, Y.M. *Stoichiometry in Crystal Compounds and Its Influence on Their Physical Properties*; Nova Science Publishers: Hauppauge, NY, USA, 1988.
26. Rowe, D.M. *Modules, Systems, and Applications in Thermoelectrics*; CRC Press: Boca Raton, FL, USA, 2012.
27. Fu, H.; Ying, P.Z.; Cui, J.L.; Yan, Y.M.; Zhang, X.J. Vacancy phonon scattering and thermoelectric properties in In_2Te_3 SnTe compounds. *Mater. Sci. Forum* **2010**, *650*, 126–131. [CrossRef]

28. Tan, G.; Zeier, W.G.; Shi, F.; Wang, P.; Snyder, G.J.; Dravid, V.P.; Kanatzidis, M.G. High thermoelectric performance SnTe-In_2Te_3 solid solutions enabled by resonant levels and strong vacancy phonon scattering. *Chem. Mater.* **2015**, *27*, 7801–7811. [CrossRef]
29. Vallem, S.; Bangera, K.V.; Shivakumar, G.K. Drastic increase in thermoelectric power factor of mixed Sb_2Te_3-In_2Te_3 thin films. *Superlattices Microstruct.* **2019**, *131*, 15–20. [CrossRef]
30. Wei, M.; Shi, X.L.; Zheng, Z.H.; Li, F.; Liu, W.D.; Xiang, L.P.; Xie, Y.S.; Chen, Y.X.; Duan, J.Y.; Ma, H.L.; et al. Directional thermal diffusion realizing inorganic Sb_2Te_3/Te hybrid thin films with high thermoelectric performance and flexibility. *Adv. Funct. Mater.* **2022**, *32*, 2207903. [CrossRef]
31. Richter, W.; Becker, C. A Raman and far-infrared investigation of phonons in the rhombohedral V_2-VI_3 compounds Bi_2Te_3, Bi_2Se_3, Sb_2Te_3 and $Bi_2(Te_{1-x}Se_x)_3$ (0<x<1), $(Bi_{1-y}Sb_y)_2Te_3$ (0<y<1). *Phys. Status Solidi (b)* **1977**, *84*, 619–628.
32. Richter, W.; Krost, A.; Nowak, U.; Anastassakis, E. Anisotropy and dispersion of coupled plasmon-LO-phonon modes in Sb_2Te_3. *Z. Krist. Phys. B Condens. Matter* **1982**, *49*, 191–198. [CrossRef]
33. Yang, H.Q.; Chen, Y.J.; Wang, X.Y.; Miao, L.; Li, X.D.; Han, X.D.; Lu, X.; Wang, G.Y.; Zhou, X.Y. Realizing high thermoelectric performance in Te nanocomposite through Sb^2Te^3 incorporation. *CrystEngComm* **2018**, *20*, 7729–7738. [CrossRef]
34. Tan, M.; Shi, X.L.; Liu, W.D.; Li, M.; Wang, Y.L.; Li, H.; Deng, Y.; Chen, Z.G. Synergistic texturing and Bi/Sb-Te antisite doping secure high thermoelectric performance in $Bi_{0.5}Sb_{1.5}Te_3$-based thin films. *Adv. Energy Mater.* **2021**, *11*, 2102578. [CrossRef]
35. Wang, Q.; Xiang, L.P.; Mei, D.; Xie, Y.S. Graphene Aerogels, Structure Control, Thermal characterization and thermal transport. *Int. J. Thermophys.* **2020**, *41*, 155. [CrossRef]
36. Xu, Z.; Xu, S.; Tang, X.; Wang, X. Energy transport in crystalline DNA composites. *AIP Adv.* **2014**, *4*, 017131. [CrossRef]
37. Guo, J.Q.; Wang, X.W.; Wang, T. Thermal characterization of microscale conductive and nonconductive wires using transient electrothermal technique. *J. Appl. Phys.* **2007**, *101*, 063537. [CrossRef]